Chapter 10

Nonlinear Radiative Heat Transfer of Cu-Water Nanoparticles over an Unsteady Rotating Flow under the Influence of Particle Shape

K. Ganesh Kumar, B.J. Gireesha and S. Manjunatha

Additional information is available at the end of the chapter

http://dx.doi.org/10.5772/intechopen.74807

Abstract

A 3D study on Cu-water-rotating nanofluid over a permeable surface in the presence of nonlinear radiation is presented. Particle shape and thermophysical properties are considered in this study. The governing equations in partial forms are reduced to a system of nonlinear ordinary differential equations using suitable similarity transformations. An effective Runge-Kutta-Fehlberg fourth-fifth order method along with shooting technique is applied to attain the solution. The effects of flow parameters on the flow field and heat transfer characteristics were obtained and are tabulated. Useful discussions were carried out with the help of plotted graphs and tables. It is found that the rate of heat transfer is more enhanced in column-shaped nanoparticles when compared to tetrahedron- and sphere-shaped nanoparticles. Higher values of rotating parameter enhance the velocity profile and corresponding boundary layer thickness. It has quite the opposite behavior in angular velocity profile. Further, unsteady parameter increases the velocity profile and corresponding boundary layer thickness.

Keywords: particle shape effect, nonlinear radiation, Cu-water nanoparticles, unsteady rotating flow

1. Introduction

The interaction of thermal radiation has increased greatly during the last decade due to its importance in many practical applications. We know that the radiation effect is important under many isothermal and nonisothermal situations. If the entire system involving the polymer extrusion process is placed in a thermally controlled environment, then radiation

could become important. The knowledge of radiation heat transfer in the system can, perhaps, lead to a desired product with a sought characteristic. Magnetohydrodynamic 3D flow of viscoelastic nanofluid in the presence of nonlinear thermal radiation has been examined by Hayat et al. [1]. Shehzad et al. [2] proposed the nonlinear thermal radiation in 3D flow of Jeffrey nanofluid. Refs. [3–11] are some of the works associated with stretching sheet problem of thermal radiation.

Nanotechnology has been widely utilized in the industries since materials with the size of nanometers possess distinctive physical and chemical properties. Nanofluids are literally a homogeneous mixture of base fluid and the nanoparticles. Common base fluids embody water, organic liquids, oil and lubricants, biofluids, polymeric solution and other common liquids. Nanoparticles are created from totally different materials, like oxides, nitrides, carbide, ceramics metals, carbons in varied (e.g., diamond, graphite, carbon nanotubes, fullerene) and functionalized nanoparticles. Nanofluids have novel properties that are potentially helpful in several applications in heat transfer, as well as microelectronics, pharmaceutical processes, heat exchanger, hybrid-powered engines, domestic refrigerator, fuel cells, cooling/vehicle thermal management, nuclear reactor agent, in grinding, in space technology, ships and in boiler flue gas temperature reduction. Choi [12] was the first who composed the analysis on nanoparticles in 1995. Later, Maiga et al. [13] initiated the heat transfer enhancement by using nanofluids in forced convective flows. The laminar fluid flow which results from the stretching of a flat surface in a nanofluid has been investigated by Khan and Pop [14]. Recently, a number of researchers are concentrating on nanofluid with different geometries; see [15–19].

Experimental studies have shown that the thermal conductivity of nanofluids is determined by the parameters related to: nanoparticles, concentration, size, spherical and nonspherical shapes, agglomeration (fractal-like shapes), surface charge and thermal conductivity, base fluids (e.g., thermal conductivity and viscosity), nanofluids (e.g., temperature), the interfacial chemical/physical effect or interaction between the particles and base fluid and others. For more details, readers are referred to the studies [20–25].

Impact of nonlinear thermal radiation on 3D flow and heat transfer of Cu-water nanoliquid over unsteady rotating flow have been considered. The heat transfer characteristics are studied in the presence of different particle shapes, thermophysical properties and nonlinear thermal radiation. The principal equations of continuity, momentum, energy and mass equations are transferred into a set of nonlinear similarity equalities by applying the appropriate transformations. The condensed equalities are solved numerically, and the impacts of relevant parameters are discussed through plotted graphs and tables.

2. Mathematical formulation

An unsteady laminar flow over a permeable surface in a rotating nanofluid is considered in this study. The copper-water motion is 3D due to Coriolis force in the present problem. The Cartesian coordinates are x, y and z where the rotation of the nanofluid is at an angular velocity $\overline{\Omega}(t)$ about the z-axis, and time is denoted as t. Let $u_w(x,t) = \frac{bx}{1-\delta t}$ and $v_w(x,t)$ represent

http://dx.doi.org/10.5772/intechopen.74807

the surface velocity in x and y directions, respectively, and $w_w(x,t)$ is the wall mass flux velocity in the z-direction as represented in **Figure 1**. Under these conditions, the governing equations can be written as:

$$\frac{\partial u}{\partial x}+\frac{\partial v}{\partial y}+\frac{\partial w}{\partial z}=0, \tag{1}$$

$$\frac{\partial u}{\partial t}+u\frac{\partial u}{\partial x}+v\frac{\partial u}{\partial y}+w\frac{\partial u}{\partial z}-2\overline{\Omega}v=-\frac{1}{\rho}\frac{\partial p}{\partial x}+\frac{\mu_{nf}}{\rho_{nf}}\frac{\partial^2 u}{\partial z^2}, \tag{2}$$

$$\frac{\partial v}{\partial t}+u\frac{\partial v}{\partial x}+v\frac{\partial v}{\partial y}+w\frac{\partial v}{\partial z}+2\overline{\Omega}v=-\frac{1}{\rho}\frac{\partial p}{\partial y}+\frac{\mu_{nf}}{\rho_{nf}}\frac{\partial^2 v}{\partial z^2}, \tag{3}$$

$$\frac{\partial w}{\partial t}+u\frac{\partial w}{\partial x}+v\frac{\partial w}{\partial y}+w\frac{\partial w}{\partial z}=-\frac{1}{\rho}\frac{\partial p}{\partial z}+\frac{\mu_{nf}}{\rho_{nf}}\frac{\partial^2 v}{\partial z^2}, \tag{4}$$

$$\frac{\partial T}{\partial t}+u\frac{\partial T}{\partial x}+v\frac{\partial T}{\partial y}+w\frac{\partial T}{\partial z}=\alpha_{nf}\frac{\partial^2 T}{\partial z^2}+\frac{1}{(\rho c_p)_{nf}}\frac{\partial q_r}{\partial z}. \tag{5}$$

Boundary conditions for the problem are,

$$\begin{aligned} &u=u_w(x,t)=v=0, w=0, T=T_w \ \text{ at } \ z=0,\\ &u\to 0, v\to 0, w=0, T\to T_\infty \ \text{ as } \ z\to\infty \end{aligned} \tag{6}$$

where velocity components in x, y and z directions are u, v and w, constant angular velocity of the Nano fluid is Ω, dynamic viscosity of the Nano fluid is μ_{nf}, density of the nanofluid is ρ_{nf}, thermal diffusivity of the nanofluid is α_{nf}, T is temperature of nanofluid and wall temperature is T_w, T_∞ denotes temperature outside the surface (**Table 1**).

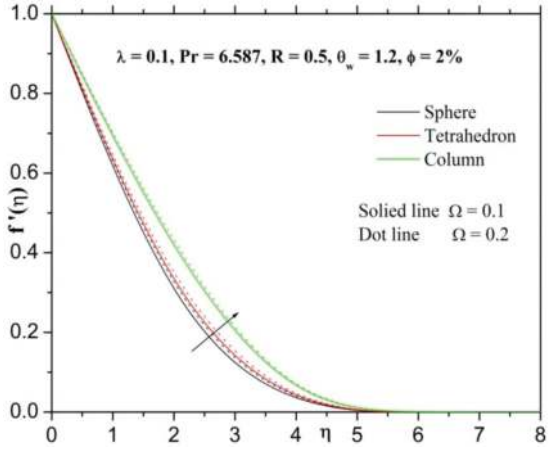

Figure 1. Influence of Ω on $f'(\eta)$.

The radiative heat flux expression in Eq. (5) is given by:

$$q_r = -\frac{16\sigma^*}{3k^*}T_\infty^3\frac{\partial T}{\partial z} \tag{7}$$

where σ^* and k^* are the Stefan-Boltzmann constant and the mean absorption coefficient, respectively, and in view to Eq. (7), Eq. (4) reduces to:

$$\frac{\partial T}{\partial t}+u\frac{\partial T}{\partial x}+v\frac{\partial T}{\partial y}+w\frac{\partial T}{\partial z}=\frac{\partial}{\partial y}\left[\left(\alpha_{nf}+\frac{16\sigma^*T_\infty^3}{3(\rho c_p)_{nf}k^*}\frac{\partial T}{\partial Z}\right)\right]\frac{\partial T}{\partial y}. \tag{8}$$

Parameters μ_{nf}, ρ_{nf} and α_{nf} are interrelated with nanoparticle volume fraction; ϕ and can be defined as:

$$\begin{aligned}&\rho_{nf}=\rho_f\left(1-\phi+\phi\left(\frac{\rho_s}{\rho_f}\right)\right),\ \mu_{nf}=\frac{\mu_f}{(1-\phi)^{2.5}},\ \alpha_{nf}=\frac{k_{nf}}{(\rho c_p)_{nf}}\\&(\rho c_p)_{nf}=(\rho c_p)_f\left(1-\phi+\phi\left(\frac{(\rho c_p)_s}{(\rho c_p)_f}\right)\right),\ \frac{k_{nf}}{k_f}=\frac{[k_s+(m-1)k_f]-(m-1)\phi(k_f-k_s)}{[k_s+(m-1)k_f]+\phi(k_f-k_s)}\end{aligned} \tag{9}$$

where volumetric heat capacity of the solid nanoparticles is $(\rho c_p)_s$, volumetric heat capacity of the base fluid is $(\rho c_p)_f$, volumetric heat capacity of the nanofluid is $(\rho c_p)_{nf}$, thermal conductivity of the nanofluid is k_{nf}, thermal conductivity of the base fluid is k_f, thermal conductivity of the solid nanoparticles is k_s, nanoparticle volume fraction is ϕ, density viscosity of the base fluid is ρ_f and dynamic viscosity of the base fluid is μ_f (**Table 2**).

Now, we introduce similarity transformations:

$$u=\frac{bx}{1-\delta t}f'(\eta),\ v=\frac{bx}{1-\delta t}g(\eta),\ w=-\sqrt{\frac{bx}{1-\delta t}}f(\eta),\ \eta=\sqrt{\frac{bx}{\upsilon(1-\delta t)}}z,\ \theta(\eta)=\frac{T-T_\infty}{T_w-T_\infty} \tag{10}$$

with $T=T_\infty(1+(\theta_w-1)\theta)$ and $\theta_w=\frac{T_w}{T_\infty}$, $\theta_w>1$ is the temperature ratio parameter.

	ρ	c_p	k
Copper (Cu)	385	8933	400
Water	997.1	4179	0.613

Table 1. Thermophysical properties of water and nanoparticles.

Particle shapes	**Sphere**	**Tetrahedron**	**Column**
m	3	4.0613	6.3698

Table 2. Values of the empirical shape factor for different particle shapes.

Using Eqs. (2)–(6) and (10), we can have

$$\frac{1}{(1-\phi)^{2.5}\left(1-\phi+\phi\left(\frac{\rho_s}{\rho_f}\right)\right)}f''' - \left[f'^2 - ff'' - 2\Omega g + \lambda\left(\frac{\eta}{2}f'' + f'\right)\right] = 0, \tag{11}$$

$$\frac{1}{(1-\phi)^{2.5}\left(1-\phi+\phi\left(\frac{\rho_s}{\rho_f}\right)\right)}g'' - \left[f'g - fg' - 2\Omega f + \lambda\left(\frac{\eta}{2}g' + g\right)\right] = 0, \tag{12}$$

$$\frac{k_{nf}}{k_f\left(1-\phi+\phi\left(\frac{(\rho c_p)_s}{(\rho c_p)_f}\right)\right)}\left[1+R(1+(\theta_w-1)\theta)^3\theta\right] - \Pr\left[\lambda\frac{\eta}{2}\theta' - f\theta'\right] = 0, \tag{13}$$

The transformed boundary conditions are as follows:

$$\begin{aligned} &f(0) = 0, f'(0) = 1, g(0) = 0, \theta(0) = 1 \text{ at } \eta = 0 \\ &f'(\eta) \to 0, g(\eta) \to 0, \theta(\eta) \to 0 \text{ as } \eta \to \infty \end{aligned} \tag{14}$$

where $\Omega = \frac{\omega}{b}$ is rotation rate, $\lambda = \frac{\delta}{b}$ is unsteadiness parameter $R = \frac{16\sigma^* T_\infty^3}{3k_f k^*}$ is radiation parameter, $\Pr = \frac{\alpha_{nf}}{\upsilon_{nf}}$ is Prandtl number and primes denote the differentiation with respect to η.

Rosca et al. [11] mentioned that the pressure term (p) can be integrated from Eq. (4); thus, we obtain:

$$p = \upsilon\rho\frac{\partial w}{\partial z} - \frac{\rho w^2}{2} + c \tag{15}$$

The physical quantities of interest in this problem are the skin friction coefficients in x and y directions, C_{fx} and C_{fy} as well as the local Nusselt number Nu_x which are defined as:

$$C_{fx} = \frac{\tau_{wx}}{\rho u_w^2(xt)},\ C_{fy} = \frac{\tau_{wy}}{\rho u_w^2(yt)},\ Nu_x = \frac{xq_w}{k_f(T_w - T_\infty)}, \tag{16}$$

Surface shear stress τ_{wx}, τ_{wy} and surface heat flux q_w are defined as:

$$\tau_{wx} = \mu_{nf}\left(\frac{\partial u}{\partial z}\right)_{z=0}, \tau_{wy} = \mu_{nf}\left(\frac{\partial v}{\partial z}\right)_{z=0} \text{ and } q_w = -k_{nf}\left(\frac{\partial T}{\partial z}\right) + qr_{z=0} \tag{17}$$

Using Eqs. (16) and (17), we obtain

$$\sqrt{\mathrm{Re}_x}C_{fx} = \frac{1}{(1-\phi)^{2.5}}f''(0),\ \sqrt{\mathrm{Re}_x}C_{fy} = \frac{1}{(1-\phi)^{2.5}}g'(0) \text{ and } \frac{Nu_x}{\sqrt{\mathrm{Re}_x}} = \frac{k_{nf}}{k_f}\left(-\left[1+R\theta_w^3\right]\theta'(0)\right), \tag{18}$$

where $\mathrm{Re}_x = \frac{u_w x}{\upsilon}$ is local Reynolds number.

3. Numerical method

Numerical solutions of nonlinear coupled differential Eqs. (11)–(13) subject to the boundary conditions (14) constitute a two-point boundary value problem. Due to coupled and highly nonlinear nature, which are not amenable to closed-form solutions; therefore, we resorted to numerical solutions. In order to solve these equations numerically, we follow most efficient fourth-fifth order Runge-Kutta-Fehlberg integration scheme along with shooting technique. In this method, it is most important to choose the appropriate finite values of η_∞. The asymptotic boundary conditions at η_∞ were replaced by those at η_8 in accordance with standard practice in the boundary layer analysis.

4. Result and discussion

To get a clear insight into the physical situation of the present problem, numerical values for velocity and temperature profile are computed for different values of dimensionless parameters using the method described in the previous section. The numerical results for the local Nusselt number are presented for different values of the governing parameters in **Table 3**.

λ	Ω	Pr	R	θ_w	ϕ.	Nusselt number		
						$m = 3$	$m = 4.0613$	$m = 6.3698$
0.2						0.36722	0.35144	0.32983
0.3						0.29671	0.29256	0.28353
0.4						0.21897	0.22635	0.23028
	0.01					0.33069	0.32112	0.30611
	0.02					0.29005	0.28739	0.27973
	0.03					0.24936	0.25364	0.25333
		5.776				0.35865	0.34247	0.32053
		6.587				0.36722	0.35151	0.32990
		7.578				0.37598	0.36090	0.33978
			0.5			0.36722	0.35144	0.32983
			1			0.33266	0.31642	0.29491
			1.5			0.30957	0.29332	0.27217
				1.2		0.36722	0.35144	0.32983
				1.4		0.32565	0.31078	0.29076
				1.6		0.28807	0.27416	0.25572
					1%	0.43665	0.42492	0.40752
					2%	0.36722	0.35144	0.32983
					3%	0.30841	0.29212	0.27084

Table 3. Numerical values of Nusselt number for different physical parameters.

http://dx.doi.org/10.5772/intechopen.74807

Figure 1 portrays the effect of Ω on velocity profile $f'(\eta)$. The velocity profile and corresponding thickness of the boundary layer enhance with larger values of Ω. This is because the larger value of Ω parameter leads to higher rotation rate as compared to stretching rate. Therefore, the larger rotation effect enhances velocity field. **Figure 2** shows the impact of Ω on angular profile $g(\eta)$. From this figure, one can see that $g(\eta)$ reduces for larger values of Ω. Further, it is noticed that rate of heat transfer is larger in column-shaped nanoparticles when compared to tetrahedron- and sphere-shaped nanoparticles.

Figures 3 and **4** depict the effect of λ on the $f'(\eta)$ and $g(\eta)$ profile. It is clear from both the figures that an increase in λ decreases the momentum boundary layer thickness resulting in velocity decrease. It is also noted that $g(\eta)$ decreases smoothly with the increase in the

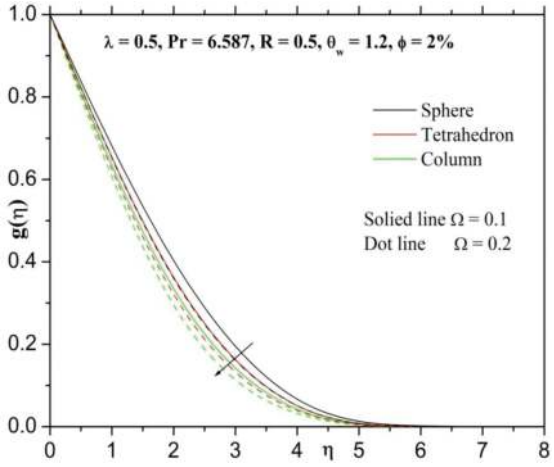

Figure 2. Influence of Ω on $g(\eta)$.

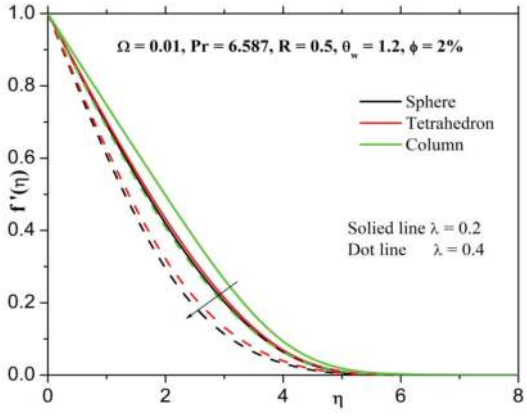

Figure 3. Influence of λ on $f'(\eta)$.

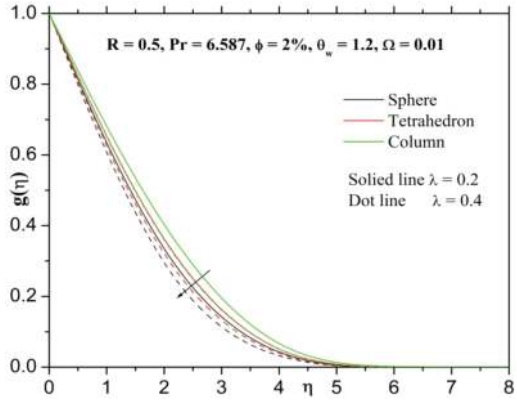

Figure 4. Influence of λ on $g(\eta)$.

unsteadiness parameter. This shows an important fact that the rate of cooling is much faster for higher values of λ, whereas it may take a longer time in steady flows.

Influence of the solid volume fraction parameter (ϕ) on temperature profiles $\theta(\eta)$ can be visualized in **Figure 5**. It is observed that the temperature profile increases by increasing values of the solid volume fraction parameter. This is due to the fact that the volume occupied by the dust particles per unit volume of mixture is higher so that it raises the rate of heat transfer. It was noticed that the development in the temperature profiles of column-shaped nanoparticles is high when compared to temperature profiles of sphere- and tetrahedron-shaped nanoparticles due to the increase in volume fraction of nanoparticles.

The effect of temperature ratio parameter (θ_w) on temperature profile is shown in **Figure 6**. The influence of temperature ratio parameter enriches the temperature profile and corresponding boundary layer thickness. This may happen due to the fact that the fluid temperature is much

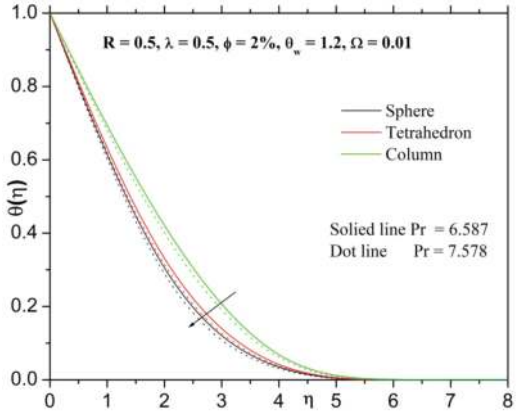

Figure 5. Influence of Pr on $\theta(\eta)$.

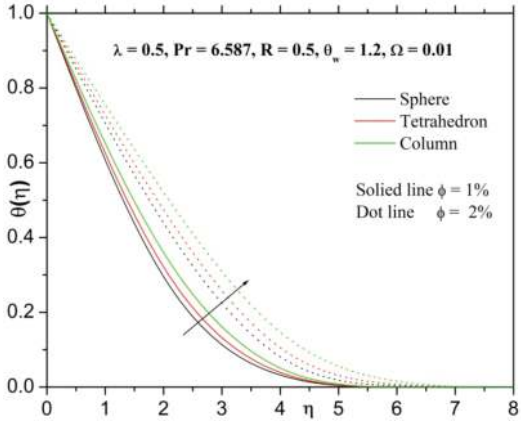

Figure 6. Influence of ϕ on $\theta(\eta)$.

higher than the ambient temperature for increasing values of θ_w, which increases the thermal state of the fluid. It is also observed that the rate of heat transfer is higher in the column-shaped nanoparticles than that of tetrahedron- and sphere-shaped nanoparticles.

Figure 7 demonstrates the effect of the Prandtl number (Pr) on temperature profiles of $\theta(\eta)$. The above mentioned graph elucidate that the temperature profile and corresponding thermal boundary layer thickness decrease rapidly with increasing values of Pr. Physically, the Prandtl number is the ratio of momentum diffusivity to thermal diffusivity. In fact, the larger Prandtl number means that the lower thermal diffusivity. A decrease in the thermal diffusivity leads to a decrease in the temperature and its associated boundary layer thickness.

The temperature distribution $\theta(\eta)$ for various values of radiation parameter (R) is shown in **Figure 8**. This figure reveals that the larger values of radiation parameter increase the temperature profile and thermal boundary layer thickness. Generally, higher values of

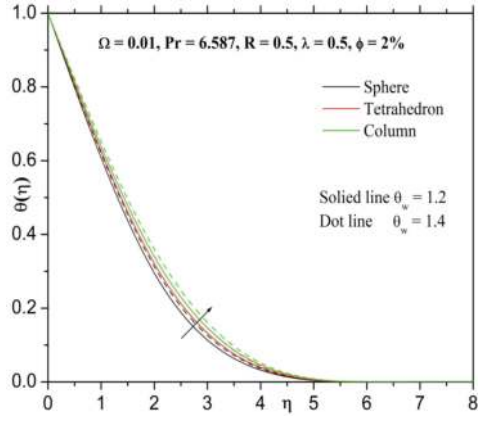

Figure 7. Influence of θ_w on $\theta(\eta)$.

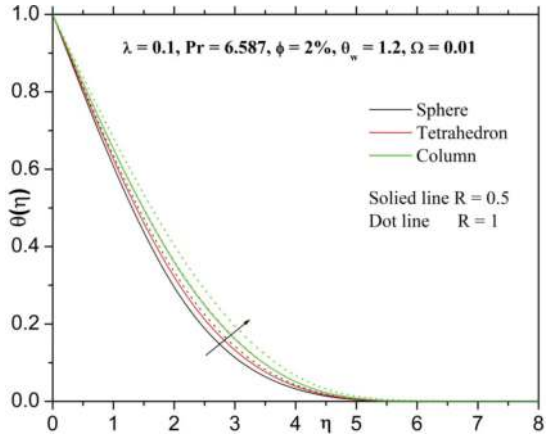

Figure 8. Influence of R on $\theta(\eta)$.

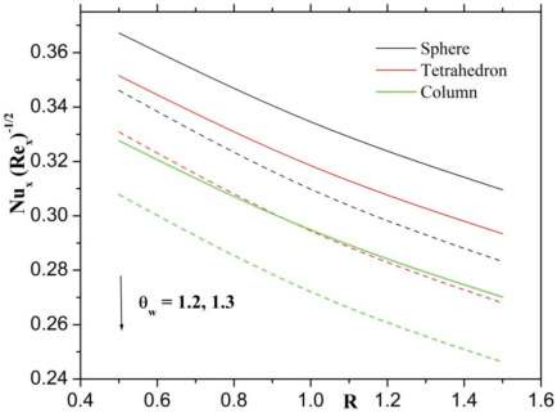

Figure 9. Influence of θ_w and R on Nusselt number.

radiation parameter produce additional heat to the operating fluid that shows associate enhancement within the temperature field. We have noticed an improvement within the temperature profile because of increase in the radiation parameter. Moreover, the rate of heat transfer at the wall is less in case of the sphere-shaped particles when compared to the tetrahedron- and column-shaped nanoparticles.

Figure 9 shows the effect of θ_w and R on the skin friction coefficient. Here, we observed that the skin friction coefficient decreases for larger values of θ_w and R. **Figure 10** delineates the influence of ϕ and Ec on Nusselt number. One can observe from the figure that Nusselt number decreases for larger values of ϕ and Ec. It is also perceived from these figures that the maximum decrease in the rate of heat transfer of nanofluid is motivated by the column-shaped, followed by

http://dx.doi.org/10.5772/intechopen.74807

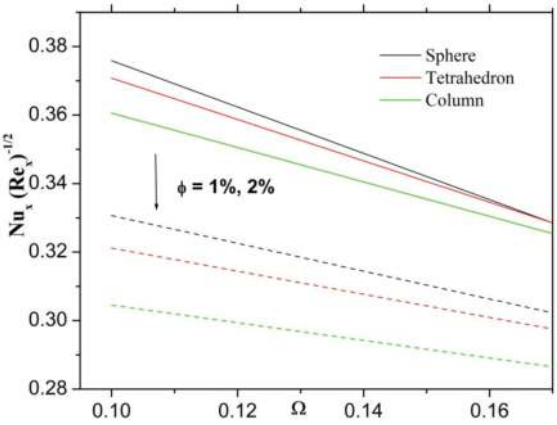

Figure 10. Influence of ϕ and Ω on Nusselt number.

tetrahedron- and sphere-shaped nanoparticles, respectively. It is just because of the nanofluid which contains column-shaped nanoparticles having maximum thermal conductivity than nanofluids containing tetrahedron- and sphere-shaped nanoparticles. **Table 3** presents the numerical values of Nusselt number for various values physical parameter values. It is observed that Nusselt number increases with increasing Pr. Further, from **Table 3**, we observe that Nusselt number decreases with increasing values of θ_w, R, ϕ and λ.

5. Conclusions

In the present analysis, impact nonlinear radiative heat transfer of Cu-water nanoparticles over an unsteady rotating flow under the influence of particle shape is considered. Effects of various parameters are studied graphically. The main points of the present simulations are listed as follows:

- The highlight of this study is that temperature profile is more enhanced in column-shaped nanoparticles when compared to tetrahedron- and sphere-shaped nanoparticles.
- Temperature profile and thermal boundary layer thickness increase with increasing values of R and θ_w.
- The thermal boundary layer thickness and temperature profile enhance with increasing values of ϕ.
- Higher values of rotating parameter enhance the velocity profile and corresponding boundary layer thickness. It has quite opposite behavior in angular velocity profile.
- Unsteady parameter increases the velocity profile and corresponding boundary layer thickness.

Author details

K. Ganesh Kumar[1], B.J. Gireesha[1] and S. Manjunatha[2]*

*Address all correspondence to: manjubhushana@gmail.com

1 Department of Studies and Research in Mathematics, Kuvempu University, Shimoga, Karnataka, India

2 Department of Engineering Mathematics, Faculty of Engineering, Christ University, Bengaluru, India

References

[1] Hayat T, Muhammad T, Alsaedi A, Alhuthali MS. Magnetohydrodynamic three-dimensional flow of viscoelastic nanofluid in the presence of nonlinear thermal radiation. Journal of Magnetism and Magnetic Materials. 2015;**385**:222-229

[2] Shehzad SA, Hayat T, Alsaedi A, Mustafa AO. Nonlinear thermal radiation in three-dimensional flow of Jeffrey nanofluid: A model for solar energy. Applied Mathematics and Computation. 2014;**248**:273-286

[3] Mustafa M, Mushtaq A, Hayat T, Alsaedi A. Radiation effects in three-dimensional flow over a bi-directional exponentially stretching sheet. Journal of the Taiwan Institute of Chemical Engineers. 2015;**47**:43-49

[4] Kafoussias NG, Williams EW. Thermal-diffusion and diffusion-thermo effects on mixed free-forced convective and mass transfer boundary layer flow with temperature dependent viscosity. International Journal of Engineering Science. 1995;**33**(9):1369-1384

[5] Srinivasacharya D, Kaladhar K. Mixed convection flow of couple stress fluid in a non-darcy porous medium with Soret and Dufour effects. Journal of Applied Science and Engineering. 2012;**15**:415-422

[6] Rudraswamy NG, Kumar KG, Gireesha BJ, Gorla RSR. Soret and Dufour effects in three-dimensional flow of Jeffery nanofluid in the presence of nonlinear thermal radiation. Journal of Nanoengineering and Nanomanufacturing. 2017;**6**(4):278-287

[7] Kumar KG, Rudraswamy NG, Gireesha BJ, Krishnamurthy MR. Influence of nonlinear thermal radiation and viscous dissipation on three-dimensional flow of Jeffrey nano fluid over a stretching sheet in the presence of joule heating. Nonlinear Engineering. 2017;**6**(3): 207-219

[8] Kumar KG, Gireesha BJ, Manjunatha S, Rudraswamy NG. Effect of nonlinear thermal radiation on double-diffusive mixed convection boundary layer flow of viscoelastic nanofluid over a stretching sheet. International Journal of Mechanical and Materials Engineering. 2017;**12**(1):18

[9] Kumar KG, Rudraswamy NG, Gireesha BJ, Manjunatha S. Nonlinear thermal radiation effect on Williamson fluid with particle-liquid suspension past a stretching surface. Results in Physics. 2017;**7**:3196-3202

[10] Makinde OD, Kumar KG, Manjunatha S, Gireesha BJ. Effect of nonlinear thermal radiation on MHD boundary layer flow and melting heat transfer of micro-polar fluid over a stretching surface with fluid particles suspension. Defect and Diffusion Forum. 2017;**378**: 125-136

[11] Rosca NC, Pop I. Mixed convection stagnation point flow past a vertical flat plate with a second order slip: Heat flux case. International Journal of Heat and Mass Transfer. 2013; **65**:102-109

[12] Choi CUS. Enhancing thermal conductivity of fluids with nanoparticles. Siginer DA, Wang HP, editors. Development and Applications of Non-Newtonian Flows. Vol. 231. MD: ASME; 1995. pp. 99-10

[13] Maiga SEB, Palm SJ, Nguyen CT, Roy G, Galanis N. Heat transfer enhancement by using nanofluids in forced convection flows. International Journal of Heat and Fluid Flow. 2005; **26**:530-546

[14] Khan W, Pop I. Boundary-layer flow of a nanofluid past a stretching sheet. International Journal of Heat and Fluid Flow. 2010;**53**(11–12):2477-2483

[15] Rudraswamy NG, Shehzad SA, Ganesh Kumar KG, Gireesha BJ. Numerical analysis of MHD three-dimensional Carreau nanoliquid flow over bidirectionally moving surface. Journal of the Brazilian Society of Mechanical Sciences and Engineering. 2017;**39**(12):5037-5047

[16] Kumar KG, Gireesha BJ, Prasannakumara BC, Ramesh GK, Makinde OD. Phenomenon of radiation and viscous dissipation on Casson nanoliquid flow past a moving melting surface. Diffusion Foundations. 2017;**11**:33-42

[17] Kumar KG, Ramesh GK, Gireesha BJ, Gorla RSR. Characteristics of Joule heating and viscous dissipation on three-dimensional flow of Oldroyd B nanofluid with thermal radiation. Alexandria Engineering Journal. 2017. DOI: 10.1016/j.aej.2017.06.006

[18] Prasannakumara BC, Gireesha BJ, Krishnamurthy MR, Kumar KG. MHD flow and nonlinear radiative heat transfer of Sisko nanofluid over a nonlinear stretching sheet. Informatics in Medicine Unlocked. 2017;**9**:123-132

[19] Kumar KG, Gireesha BJ, Prasannakumara BC, Makinde OD. Impact of chemical reaction on marangoni boundary layer flow of a Casson nano liquid in the presence of uniform heat source sink. Diffusion Foundations. 2017;**11**:22-32

[20] Ellahi R, Zeeshan A, Hassan M. Shape effects of nanosize particles in Cu-H_2O nanofluid on entropy generation. International Journal of Heat and Mass Transfer. 2015;**81**:449-456

[21] Ghosh MM, Ghosh S, Pabi SK. Effects of particle shape and fluid temperature on heat-transfer characteristics of nanofluids. Journal of Materials Engineering and Performance. 2013;**22**(6):1525-1529

[22] Jeong J, Li C, Kwon Y, Lee J, Kim SH, Yun R. Particle shape effect on the viscosity and thermal conductivity of ZnO nanofluids. International Journal of Refrigeration. 2013; **36**(8):2233-2241

[23] Timofeeva EV, Routbort JL, Singh D. Particle shape effects on thermophysical properties of alumina nanofluids. Journal of Applied Physics. 2009;**106**(1):014304-1-014304-10

[24] Ji Y, Wilson C, Chen H, Ma H. Particle shape effect on heat transfer performance in an oscillating heat pipe. Nanoscale Research Letters. 2011;**6**:296

[25] Sheikholeslami M, Gorji-Bandpay M, Ganji DD. Investigation of nanofluid flow and heat transfer in presence of magnetic field using KKL model. Arabian Journal for Science and Engineering. 2014;**39**(6):5007-5016